# USE OF $^{18}$FDG-PET IMAGING TO PREDICT TREATMENT RESPONSE TO IGF-1R/IR TARGETED THERAPY IN LUNG CANCER

By

Eliot T. McKinley

Thesis

Submitted to the Faculty of the

Graduate School of Vanderbilt University

in partial fulfillment of the requirements

for the degree of

MASTER OF SCIENCE

in

Biomedical Engineering

May, 2011

Nashville, Tennessee

Approved:

H. Charles Manning, Ph.D.

Adam Anderson, Ph. D.

ACKNOWLEDGEMENTS

I would like to thank the Department of Biomedical Engineering and the Vanderbilt University Institute of Imaging Science for providing me with the teaching assistantships, research assistantships, didactic classwork, and research training to complete these studies.

My advisor, Charles Manning, has been integral to all of my development as a scientist. I am greatly indebted to all those who have helped me obtain results in this study especially Ping Zhao, Saffet Guleryuz, Joe Bugaj, Praffula Gokhale, Christine Mantis, and everyone else in the Manning group and at VUIIS.

Of course I could have never made it to this point without the support of my family and friends. My parents have always supported me in whatever endeavor I have chosen and to them I am incalculably grateful. And of course Huong, whenever I got frustrated with work, I just remembered that your work in medical school was orders of magnitude more stressful than mine, and that you are oftentimes right.

I have to credit Mr. Mark Bach and Dr. Phil Sticksel for, in large part, influencing my decision to become a scientist way back in 4$^{th}$ grade.

TABLE OF CONTENTS

Page

LIST OF TABLES

Table

LIST OF FIGURES

# LIST OF ABBREVIATIONS

| | |
|---|---|
| %ID/g | Percent injected dose per gram |
| $^{18}$FDG | 2-deoxy-2-($^{18}$F)fluoro-D-glucose |
| $^{18}$FLT | 3'-deoxy-3'[$^{18}$F]-fluorothymidine |
| BLI | Bioluminescence imaging |
| CT | Computed Tomography |
| IGF-1R | Insulin-like growth factor-1 receptor |
| IR | Insulin receptor |
| MRI | Magnetic Resonance Imaging |
| MRS | Magnetic Resonance Spectroscopy |
| OSEM | Ordered subsets expectation maximization |
| PD | Pharmacodynamic |
| PET | Positron Emission Tomography |
| PI3K | PI3-kinase |
| SH2 | Src homology 2 |
| SPECT | Single Photon Emitted Computed Tomography |
| SUV | Standardized uptake value |
| TK1 | Thymidine Kinase 1 |
| TSPO | Translator protein |

# CHAPTER I

# INTRODUCTION

## I.1 Overview of Molecular Imaging

Since the discovery of X-Rays by Wilhelm Conrad Röntgen in 1895, medical imaging has become a powerful clinical tool in the diagnosis and treatment of disease. Planar X-Ray, Computed Tomography (CT), Magnetic Resonance Imaging (MRI), and ultrasound imaging have become ubiquitous in the clinical setting. However, these modalities have until recently been limited to use as anatomical imaging modalities, i.e. imaging of structure rather than biological function. Molecular imaging, “the visualization, characterization and measurement of biological processes at the molecular and cellular levels in humans and other living systems” (1) has recently emerged as a clinical and research tool to interrogate functional biological processes. Molecular imaging can be utilized in the detection, diagnosis and prognosis of disease as well as to aid in the determination of treatment response.

The most important component of molecular imaging is the molecular imaging agent itself which is composed of two basic parts, the targeting moiety and the signaling moiety (2). The targeting moiety directs the probe to the biological target of interest. A number of types of targeting moieties are currently in use including antibodies, proteins, peptides, and small molecules. The signaling moiety provides a means for detection of the molecular imaging probe by an imaging system. Signaling moieties include

radionuclides, fluorophores, hyperpolarized molecules, nanoparticles, microbubbles and even endogenous substances.

The ability to label a targeting moiety with many types of signaling moieties allows molecular imaging to occur across a number of imaging modalities (3). The most common clinical molecular imaging modalities are Positron Emission Tomography (PET) and Single Photon Emitted Computer Tomography (SPECT), which utilize radionuclides as signaling moieties. PET imaging with positron emitting radionuclides such as $^{11}C$, $^{18}F$, $^{64}Cu$, and $^{68}Ga$ allows imaging resolutions on the order of millimeters with very high sensitivity in both clinical and preclinical settings. SPECT imaging utilizes radionuclides that exhibit a single photon decay including $^{99m}Tc$, $^{123}I$, $^{111}In$, and $^{177}Lu$. SPECT has somewhat lower sensitivity compared to PET and has lower resolution in the clinical setting, but can have higher resolution in pre-clinical imaging due to specialized hardware for small animal imaging. Fluorescence imaging with fluorescent dyes, proteins, or quantum dots can have both high sensitivity and resolution when not obscured by overlying tissues. However, it can quickly lose both when tissue is present between the fluorophore and the detector due to scattering and absorbance of the incident and fluorescent photons, as well as the presence of autofluorescence in the tissue. In practice, fluorescence imaging is mainly limited to pre-clinical imaging due to depth of detection issues. However fluorescence can be effectively utilized in superficial or topical applications in humans. Bioluminescent imaging (BLI), a purely preclinical imaging modality, utilizes reporter genes typically expressing luciferase, which cleaves injected luciferin leading to the release of light. BLI can have very high sensitivity due to the lack of naturally occurring light sources, but has roughly millimeter resolution due to

| Modality | Signal | Clinical | Sensitivity* | Resolution Clinical; Pre-Clinical |
|---|---|---|---|---|
| PET | $^{11}C$, $^{18}F$, $^{64}Cu$, $^{68}Ga$ | Yes | 1 | ~4 mm; ~2 mm |
| SPECT | $^{99m}Tc$, $^{123}I$, $^{111}In$, $^{177}Lu$ | Yes | $10^{-1}$-$10^{-2}$ | 6-8 mm; 1-2 mm |
| Fluorescence | Fluorescent proteins, fluorochromes, quantum dots | Potential | $10^{-2}$-1† | N/A; 1-3 mm |
| BLI | Light | No | 1-$10^{2}$ † | N/A; 1-10 mm |
| MRI | Gadolinium, SPIO, USPIO, $^{19}F$ | Potential | $10^{-5}$ | 1 mm; 80-100 μm |
| MRS | Endogenous compounds, hyperpolarized $^{13}C$ | Yes | < $10^{-5}$ | ~1mm; < 1mm |
| Ultrasound | Microbubbles | Potential | > $10^{-5}$ | 300-500 μm; 50 μm |
| * Relative to PET, † Depth-dependent<br>Adapted from (*2, 3*) | | | | |

scattering and absorbance of light while traveling though tissue. MRI, while typically used for anatomical imaging, may be used as a molecular imaging modality. Signaling moieties containing metals that effect either the $T_1$ or $T_2$ relaxation times of hydrogen such as Gadolinium or superparamagnetic iron oxide particles, or imaging $^{19}F$ rather than hydrogen have been developed. However, each exhibit very low sensitivity compared to PET. Additionally, Magnetic Resonance Spectroscopy (MRS) may be utilized to assay naturally occurring molecules or to detect exogenous molecules that induce chemical shift, however MRS is very low sensitivity with low resolution compared to MRI. Finally, ultrasound imaging can be used as a molecular imaging modality by the use of targeted microbubbles. Tiny gas-containing bubbles on the order of microns in diameter are injected into the blood stream and can hone to various intravascular

targets. Real time imaging ability makes ultrasound attractive for molecular imaging. However, as well as relatively high resolution in pre-clinical settings, however the sensitivity is low compared to PET, limited to intravascular targets, and has not been extensively studied as a molecular imaging modality in a clinical setting. A comparison of the performance and characteristics of these imaging modalities can be found in Table 1.

### I.2 Basics of PET imaging

PET has become a powerful clinical and research tool in oncology, neurosciences, cardiology, and pharmacology in both small animals and humans. PET detects paired gamma rays that are produced following the positron emission decay of a radionuclide tracer. The 511 keV gamma rays are emitted at almost 180º and are detected by a ring of scintillators. Detection of two scintillation events within a short time window on opposite sides of the detector ring defines a line of response within which the positron annihilation is assumed to have taken place. Based upon the detection of millions of annihilation events, an image of the radiotracer distribution can be reconstructed via a number of algorithms.

Compared to many other in vivo imaging modalities, PET has the distinct advantage of being inherently quantitative. After calibration, the radioactivity in each voxel can be determined using a number of well-established methods. While inspection of PET images can be used for simple detection of tumors, especially clinically, it is difficult to make comparisons across subjects due to differences in windowing of the images, injected dose, and various physiological factors. Study design for PET

generally breaks down in to two categories, static methods and kinetic methods. In static PET imaging, the radiotracer is injected into the patient or animal, allowed to circulate, and imaged after the tracer has reached steady state in the tissue of interest. Typically, quantification is normalized to the injected activity and the weight of the patient, and is expressed as either percent injected dose per gram (%ID/g) or as standardized uptake value (SUV). In dynamic imaging, the radiotracer is infused into the subject while in the scanner and the uptake of the tracer can be followed until it reaches a steady state level. Time-activity curves are then generated for each tissue of interest and applied either to compartment modeling or graphical analysis to determine a wide array of biologically relevant parameters. Typically, due to longer imaging times and the need to collect blood samples, dynamic imaging is typically utilized only in research studies requiring absolute quantification.

### I.3 2-deoxy-2-($^{18}$F)fluoro-D-glucose ($^{18}$FDG)

$^{18}$FDG is the only clinically approved PET tracer currently available for routine cancer detection and diagnosis. Essentially, a glucose molecule labeled with $^{18}$F at the 2' position instead of a normal hydroxyl group (4), $^{18}$FDG enters a cell via the same biochemical mechanisms as glucose through specialized glucose transporters, which are commonly elevated in cancer cells. However, once entering the cell $^{18}$FDG, like glucose, is phosphorylated by hexokinase and is trapped in the cell. However, $^{18}$FDG cannot proceed with further glycolysis, due to the functionalization with $^{18}$F at the 2' position. Image contrast arrises due to the increased glucose metabolism in neoplastic tissue compared to normal tissue and the resulting differential accumulation of trapped

probe. Imaging with $^{18}$FDG exhibits some drawbacks such as elevated uptake in inflammation as well as non-neoplastic tissues of high glucose metabolism including the heart, muscles and brain. Additionally, the cellular glycolysis pathway is a complicated biological process that can have non-intuitive effects on $^{18}$FDG uptake, especially in an anti-cancer treatment setting. One must be aware of these effects when interpreting $^{18}$FDG-PET imaging.

### I.4 Summary

While molecular imaging is a rapidly emerging tool in the clinic, by far the most common modality and molecular probe are PET and $^{18}$FDG, respectively. The work contained herein describes the application of $^{18}$FDG-PET imaging to a preclinical mouse model of human lung cancer. While other modalities could have been used for this study, $^{18}$FDG-PET imaging was chosen so as to expedite the translation of from pre-clinical imaging to human imaging.

# CHAPTER II

# $^{18}$FDG-PET PREDICTS PHARMACODYNAMIC RESPONSE TO OSI-906, A DUAL IGF-1R/IR INHIBITOR IN PRECLINICAL MOUSE MODELS OF LUNG CANCER

## II.1 Abstract

**Purpose:** To evaluate 2-deoxy-2-[$^{18}$F]fluoro-D-glucose positron emission tomography imaging ($^{18}$FDG-PET) as a predictive, non-invasive, pharmacodynamic (PD) biomarker of response following administration of a small-molecule IGF-1R/IR inhibitor, OSI-906.

**Experimental Design:** *In vitro* uptake studies of $^{3}$H-2-deoxy glucose following OSI-906 exposure were performed evaluating correlation of dose with inhibition of IGF-1R/IR as well as markers of downstream pathways and glucose metabolism. Similarly, *in vivo* PD effects were evaluated in human tumor cell line xenografts propagated in athymic nude mice by $^{18}$FDG-PET at 2, 4, and 24 hours following a single treatment of OSI-906 for the correlation of inhibition of receptor targets and downstream markers.

**Results:** Uptake of $^{3}$H-2-deoxy glucose and $^{18}$FDG was significantly diminished following OSI-906 exposure in sensitive tumor cells and subcutaneous xenografts (NCI-H292) but not in an insensitive model lacking IGF-1R expression (NCI-H441). Diminished pharmacodynamic $^{18}$FDG-PET collected immediately following the initial treatment agreed with inhibition of pIGF-1R/pIR, reduced PI3K and MAPK pathway activity, and predicted tumor growth arrest as measured by high-resolution ultrasound imaging.

**Conclusion:** $^{18}$FDG-PET appears to serve as a rapid, non-invasive, PD marker of IGF-1R/IR inhibition following a single dose of OSI-906 and should be explored clinically as a predictive clinical biomarker in patients undergoing IGF-1R/IR-directed cancer therapy.

## II.2 Introduction

The insulin-like growth factor-1 receptor (IGF-1R) is a tetrameric transmembrane receptor tyrosine kinase that is widely expressed in normal human tissues and is up-regulated in a number of human cancers including colorectal, non-small cell lung, ovarian and pediatric cancers. The receptor is composed of two α and two β subunits linked by disulfide bonds in which the extracellular α subunit is responsible for ligand binding and the β subunit consists of a transmembrane domain and a cytoplasmic tyrosine kinase domain. Ligand binding activates the tyrosine kinase activity of IGF-1R and results in trans-β subunit autophosphorylation and stimulation of signaling cascades that include PI3K-mTOR and MAPK pathways. Activation of IGF-1R has been reported to stimulate proliferation, survival, transformation, metastasis and angiogenesis, whereas inhibition of IGF-1R has been shown to impede tumorigenesis in several human xenograft models (5).

Increased expression of IGF-1R and its cognate ligands, IGF-I and IGF-II has been demonstrated in a wide range of solid tumors and hematologic neoplasias relative to normal tissue levels. Epidemiologic studies have shown an increased risk for the development of colon, lung, breast and bladder cancers with increased circulating levels of IGF-I (6-9). Additionally, IGF-1R expression levels have been correlated to poor

prognosis in renal cell carcinoma(10, 11). IGF-1R signaling mechanism has also been linked to resistance to various anti-tumor therapies including epidermal growth factor receptor inhibitors (5, 10, 12, 13).

Similarly, the insulin receptor (IR) is composed of a heterotetramer consisting of two extracellular α -subunits and two transmembrane β -subunits. Binding of insulin to the IR extracellular α-subunit causes a conformational change bringing together the two β-subunits. Activated IR tyrosine kinase phosphorylates several intracellular substrates including IRS-1-4, Shc, Gab1 and Cbl. These phosphorylated proteins provide a docking site for effector proteins containing Src homology 2 (SH2) domains further linking IR to PI3-kinase (PI3K) via the regulatory p85 subunit. Homology between IR and IGF-IR ranges from 45-65% in the ligand binding domains to 60-85% in tyrosine kinase domains. Expression of IR is highest in adipose tissue and to a lesser extent in liver, heart and muscle (14). Overexpression of IR in breast, colon, lung, ovarian and thyroid cancers suggest a role of IR in tumor progression (14). More recently it has been shown that forced overexpression of IR is tumorigenic in mice (15).

OSI-906 is a potent and highly selective tyrosine kinase inhibitor that exhibits similar biochemical potency against IGF-1R (8 nM) and IR (14 nM) and is greater than 4 orders of magnitude more selective for IGF-1R/IR compared to a wide number of other receptor and non-receptor kinases (16). Within a panel of >180 kinases only IGF-1R and IR were inhibited by greater than 50% at 1.0 μM OSI-906. Inhibition of cell proliferation and induction of apoptosis following exposure to OSI-906 appears to be directly linked to inhibition of AKT in colorectal, lung, and pancreatic cancer cell lines (5, 16). In addition, OSI-906 has shown potent antitumor activity in vivo in several xenograft

models (5). Since IGF-1R and IR pathway signaling is linked to glucose metabolism, we asked whether $^{18}$FDG-PET could function as a surrogate pharmacodynamic marker for OSI-906. To this end, we employed in vitro cell culture assays and in vivo animal models measuring uptake of radioactive glucose analogues as a function of treatment by OSI-906. Our data demonstrate that glucose uptake is rapidly inhibited in vitro and in vivo and tracks with IGF-1R, IR and AKT inhibition after OSI-906 treatment in sensitive tumors. Moreover, reduced glucose uptake was readily observed after OSI-906 treatment in tumor tissues using $^{18}$FDG-PET imaging methodologies. Hence, $^{18}$FDG-PET may function as a rapid, non-invasive tumor specific pharmacodynamic (PD) marker for OSI-906 in the clinical setting where accurate assessment of PD effects is often times limited by the lack of readily accessible tumor samples. As such $^{18}$FDG-PET may be a useful clinical tool in identifying active doses and patients potentially sensitive to this novel antitumor agent warranting further clinical investigation of this approach.

## II.3 Materials and Methods

### II.3.1 Immortal Human Lung Cancer Cell Lines

Human non-small cell lung carcinoma cell lines (NCI-H292, NCI-H441) were obtained from American Type Culture Collection (Manassas, VA). All cell lines were maintained in RPMI 1640 media (Mediatech, Manassas, VA) supplemented with 10% FBS (Sigma, St. Louis, MO) and 1% sodium pyruvate (Mediatech, Manassas, VA) and maintained at 37°C and 5.0% $CO_2$. Cells were propagated to 80-90% confluency prior to in vitro and in vivo assays.

### II.3.2 $^{3}$H-2-Deoxy Glucose *In Vitro* Uptake Assay

Cells were seeded in 12-well tissue culture plates (Becton Dickinson, Franklin Lakes, NJ) at a density of 9.0 x $10^5$ cells per well in normal glucose (11.1 mM) media and allowed to attach for 6-8 hours at 37°C (n = 3 wells/group). The media was then changed to 5.5 mM glucose media and the cells were allowed to equilibrate overnight. Three hours prior to the assay, the media was again removed and replaced with media containing 0.0 mM glucose (glucose starvation). The cells were then treated with varying concentrations of OSI-906 (0.0 μM to 30 μM) and 0.15 mCi of $^3$H-2-deoxy glucose (Perkin Elmer, Boston, MA). After 30 minutes the media was removed, the cells placed on ice and washed once with ice cold PBS (Mediatech, Manassas, VA). The PBS was then removed and the cells were lysed in RIPA buffer (Sigma, St. Louis, MO) for 15 minutes on ice. The lysates were harvested and counted in a Beckman LS6500 Liquid Scintillation counter (Fullerton, CA). $^3$H-2-deoxy glucose uptake was calculated as raw counts and normalized to control samples (0.0 μM OSI-906). As a positive control of glucose uptake inhibition, NCI-H292 cells were treated with increasing concentrations (2.5 μM – 10 μM) of cytochalasin B (Sigma, St. Louis, MO), a known inhibitor of GLUT1 and GLUT4 glucose transporters.

**II.3.4 Mouse Models**

Studies involving mice were conducted in accordance with federal and institutional guidelines. NCI-H292 and NCI-H441 non-small cell human xenograft tumors were generated as described (17). Briefly, 4 x $10^6$ cells were injected subcutaneously on the right flank of 5-6 week old female athymic nude mice (Charles Rivers, Wilmington, MA). Using this method, palpable tumors were typically observed within 2 weeks following injection of cells and were allowed to progress until approximately 150-200

$mm^3$, and then randomized for treatment studies. Measurement of volume was performed using high resolution ultrasound imaging as described (18). Mice were treated when the tumors reached ~200 $mm^3$ in volume. Blood glucose was measured using a Freestyle digital glucose meter and test strips (Abbott) before and at 2, and 4 hours after treatment with 60 mg/kg OSI-906 or 25 mM tartaric acid vehicle.

**II.3.5 Procurement of $^{18}$FDG**

$^{18}$FDG was synthesized in the Vanderbilt University Medical Center Radiopharmacy and distributed by PETNET. The average radiochemical purity of the product was 98.5% and specific activity was >1,000 Ci/mmol.

**II.3.6 $^{18}$FDG-PET Imaging**

Animal handling methods in preparation for and during $^{18}$FDG-PET imaging were similar to published protocols (19-21). Briefly, prior to imaging, mice were fasted overnight and allowed to acclimate to the PET imaging facility environment for at least 1 hour while in a warmed chamber at 31.5 $^0$C. Mice were administered a single dose of OSI-906 at 60 mg/kg in a 25 mM tartaric acid vehicle via oral gavage (n=8/group). $^{18}$FDG was administered via a single retro orbital injection of ~200 μCi (100 μL) and imaged 2, 4 and 24 hours post dosing of OSI-906, or 4 hours after tartaric acid vehicle. Mice were conscious during the uptake period and maintained in a warmed chamber. Following a 50-minute uptake period, 10-minute static PET scans were collected on a Concorde Microsystems micro-PET Focus 220 (Siemens, Culver City, CA). Mice were maintained under 2% isofluorane anesthesia in 100% $O_2$ at 2 L/min and kept warm via a circulating water heating for the duration of the scan. Immediately following imaging, mice were sacrificed and tissues collected for molecular analysis. PET images were

reconstructed using the ordered subsets expectation maximization (OSEM) algorithm. The percent injected-dose per gram of tissue (%ID/g) was calculated from analysis of tumor regions of interest using ASIPro software (Concorde Microsystems Inc.).

### II.3.7 Statistical Analysis

Wilcoxon Rank Sum tests were performed to compare each treatment time point to vehicle treated mice. Comparisons were unadjusted for the multiplicity of testing and were deemed significant if $p < 0.05$.

### II.3.8 Pharmacokinetic Analysis

At 2, 4, and 24 hours after administration of OSI-906 blood was collected via cardiac puncture and placed in BD Microtainer EDTA collection tubes (Becton Dickinson, Franklin Lakes, NJ). The samples were centrifuged at 1500 x g for 10 minutes and plasma protein precipitated with methanol. Analysis of drug concentration was performed by HPLC-MS tandem mass spectroscopy (Applied Biosystems, Foster City, CA).

### II.3.9 Western Blot Analysis

Phosphorylation of IGF-1R and IR in cells and tumor samples were analyzed by immunoprecipitation/Western blotting. Cells were lysed using NP-40 lysis buffer (Sigma, St. Louis, MO). Tumor samples were homogenized using Precellys 24 (MO BIO Laboratories Inc., Carlsbad, CA) in tumor lysis buffer (1% Triton X-100, 10% glycerol, 50 mM HEPES (pH 7.4), 150 mM NaCl, 1.5 mM $MgCl_2$, 1 mM EDTA supplemented with fresh protease inhibitor cocktail (Sigma, St. Louis, MO), phosphatase inhibitor cocktail (Sigma, St. Louis, MO), 10 mM NaF and 1 mM sodium orthovanadate). After pre-clearing by centrifugation (14,000 rpm for 15 minutes), 1 mg of total protein was

immunoprecipitated with anti-phosphotyrosine antibody (pY20, Exalpha, Shirley, MA) at 4 $^{0}$C overnight. The immunoprecipitates were separated on SDS-PAGE and immunoblotted with a total IGF-1R antibody (Cell Signaling, Danvers, MA) followed by detection using enhanced chemiluminesence (GE Healthcare Life Sciences, Piscataway, NJ). The blots were re-probed with total IR antibody (Cell Signaling, Danvers, MA). Phosphorylated IGF1-R and IR bands were quantified using an Image Quant LAS 4000 with Image Quant TL 7.0 software (GE Healthcare Life Sciences, Piscataway, NJ).

Markers of altered glycolysis were analyzed by Western blot analysis. Tumor or cell lysate samples were separated on SDS-PAGE, immunoblotted and detected using enhanced chemiluminesence (GE Healthcare Life Sciences, Piscataway, NJ). The antibodies included pAKT (Ser473), total AKT, pS6 (Ser235/236), pERK 1/2, total ERK 1/2, (Cell Signaling, Danvers, MA) and β-actin (Sigma, St. Louis, MO). The phosphorylated to total signal intensities were quantified as above.

**II.3.10 RTK Analysis**

Tumor lysates were prepared according to manufactures protocol (Proteome Profiler, R&D Systems, Minneapolis, MN) in NP-40 lysis buffer and clarified by centrifugation. The samples were incubated with the Human Phospho-RTK Array at 2000 µg total protein overnight at 4 $^{0}$C with rocking. The arrays were developed using Super- Signal FEMTO ECL detection (Pierce, Rockford, IL). The phospho-spots on the RTK blot were quantified using Image Quant LAS 4000 with Image Quant TL 7.0 software (GE Healthcare Life Sciences, Piscataway, NJ)

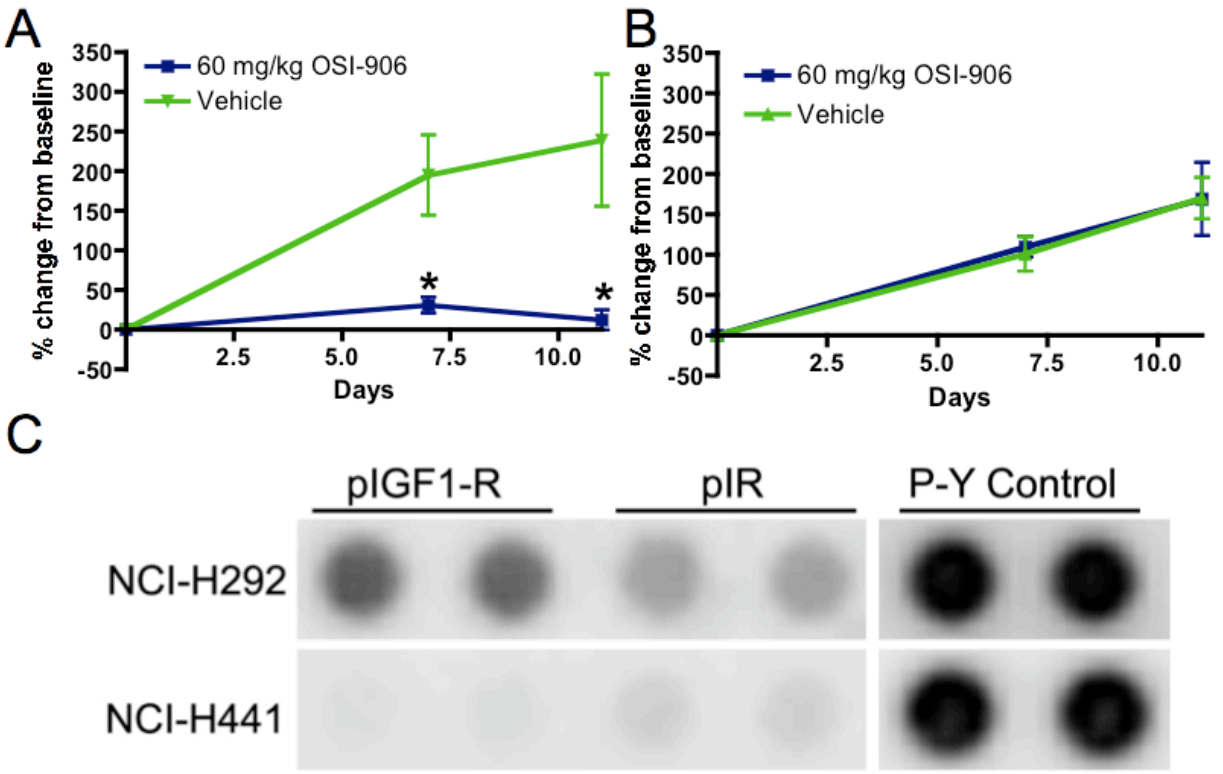


**F Fig. 1 Validation of cell lines.** Daily treatment of mice bearing NCI-H292 xenografts with 60 mg/kg OSI-906 results in significant tumor growth inhibition (A) compared to analogously treated vehicle controls. In contrast, NCI-H441 xenografts (B) do not exhibit a difference in tumor growth when comparing OSI-906-treated and vehicle-treated cohorts. Receptor tyrosine kinase (RTK) arrays (C), illustrate that NCI-H292 cells possess relatively high levels of pIGF-1R and pIR compared to the barely detectable levels of pIGF-1R and pIR in NCI-H441 cells.

## II.4 Results

### II.4.1 Sensitivity of Xenograft Models to OSI-906

Non-small cell lung cancer is a potentially attractive indication for OSI-906 due to the implication of IGF1R/IR as a driver in this, as well as drug resistance in this setting. We established sensitivity of the NCI-H292 and NCI-H441 xenograft models to OSI-906 in vivo by measuring tumor volumes longitudinally with high resolution ultrasound imaging. Daily treatment with 60 mg/kg OSI-906 over 10 days resulted in tumor growth inhibition in the NCI-H292 xenografts compared to controls (Fig. 1A), but no growth

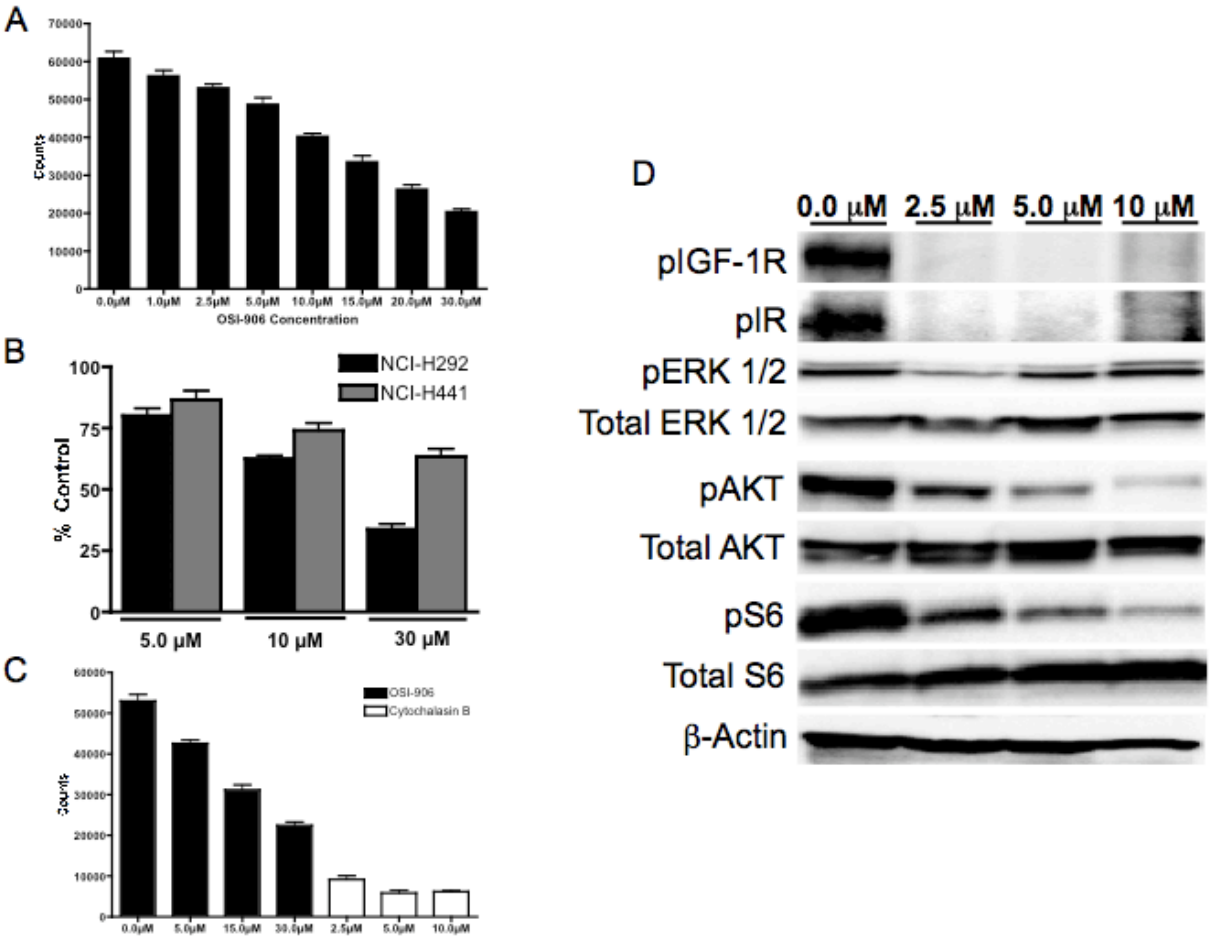


**Fig. 2. *In vitro* treatment response.** $^{3}$H-2-deoxy glucose uptake 30 minutes after OSI-906 treatment in NCI-H292 cells showed a dose-dependent decrease (A). Similar decreases in $^{3}$H-2-deoxy glucose uptake were seen at higher doses of OSI-906 in the non responding NCI-H441 cells compared with the responding NCI-H292 cells (B). Treatment with cytochalasin B as a positive control in NCI-H292 cells demonstrated that $^{3}$H-2-deoxy glucose uptake is directly affected by exposure OSI-906, and can be linked directly to cellular pathways associated with glucose metabolism (C). Western blot of NCI-H292 cells following 30 minutes of exposure to OSI-906 shows target inhibition of pIGF-1R and pIR at all doses as well as inhibition of downstream targets pAKT and pS6 (D).

changes were observed in the non-responsive NCI-H441 xenografts (Fig. 1B). We found that NCI-H292 tumors had considerably higher levels of pIGF-1R and pIR than NCI-H441 tumors (Fig. 1C).

### II.4.2 Inhibition of $^{3}$H-2-Deoxy glucose uptake *in vitro*

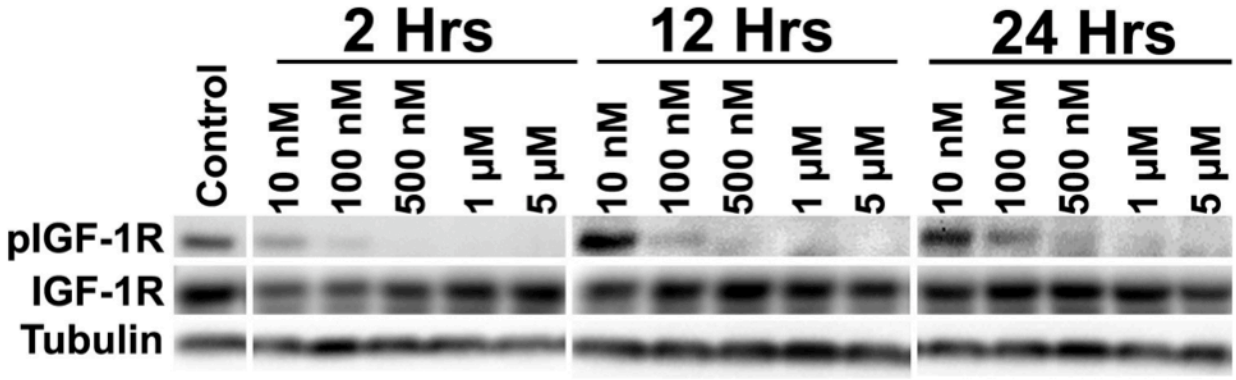


**Fig. 3. *In Vitro* treatment time course.** Western blot of NCI-H292 cells treated with 10nM, 100 nM, 500 nM, 1 μM, and 5 μM OSI-906 show target inhibition over a 24 hour time course. All concentrations of OSI-906 induce a reduction in pIGF-1R at 2 hours, and inhibition remains through 24 hours in all but the lowest, 10 nM concentration.

We assessed the effect of OSI-906 treatment on uptake of $^{3}$H-2-deoxy glucose in NCI-H292 and NCI-H441 cells in vitro. Cells were treated for only 30 minutes with OSI-906 in order to avoid potential anti-proliferative effects of the drug to interfere with this endpoint analysis. OSI-906 treatment resulted in a rapid and dose dependent inhibition of uptake of the radiotracer in the NCI-H292 cell line (Fig. 2A). The percent inhibition ranged from 12% to 60% as the dose increased from 1.0 μM to 30 μM OSI-906. In comparison the NCI-H441 cell line demonstrated a reduced sensitivity to OSI-906. For the NCI-H292 cell line a 35% decrease in uptake of $^{3}$H-2-deoxy glucose was achieved at 10 μM OSI-906 whereas in the NCI-H441 cell line the same decrease of the radiotracer was observed at only 30 μM OSI-906 (Fig. 2B). Analysis for cell death by FACS using the Invitrogen Live/Dead assay determined no significant cell death at all OSI-906 concentrations (1.0 μM -30 μM) tested compared to 0.05% DMSO controls (data not shown). As a positive control, cytochalasin B (2.5 μM-10 μM) was administered to the NCI-H292 cells and evaluated for $^{3}$H-2-deoxy glucose uptake in an

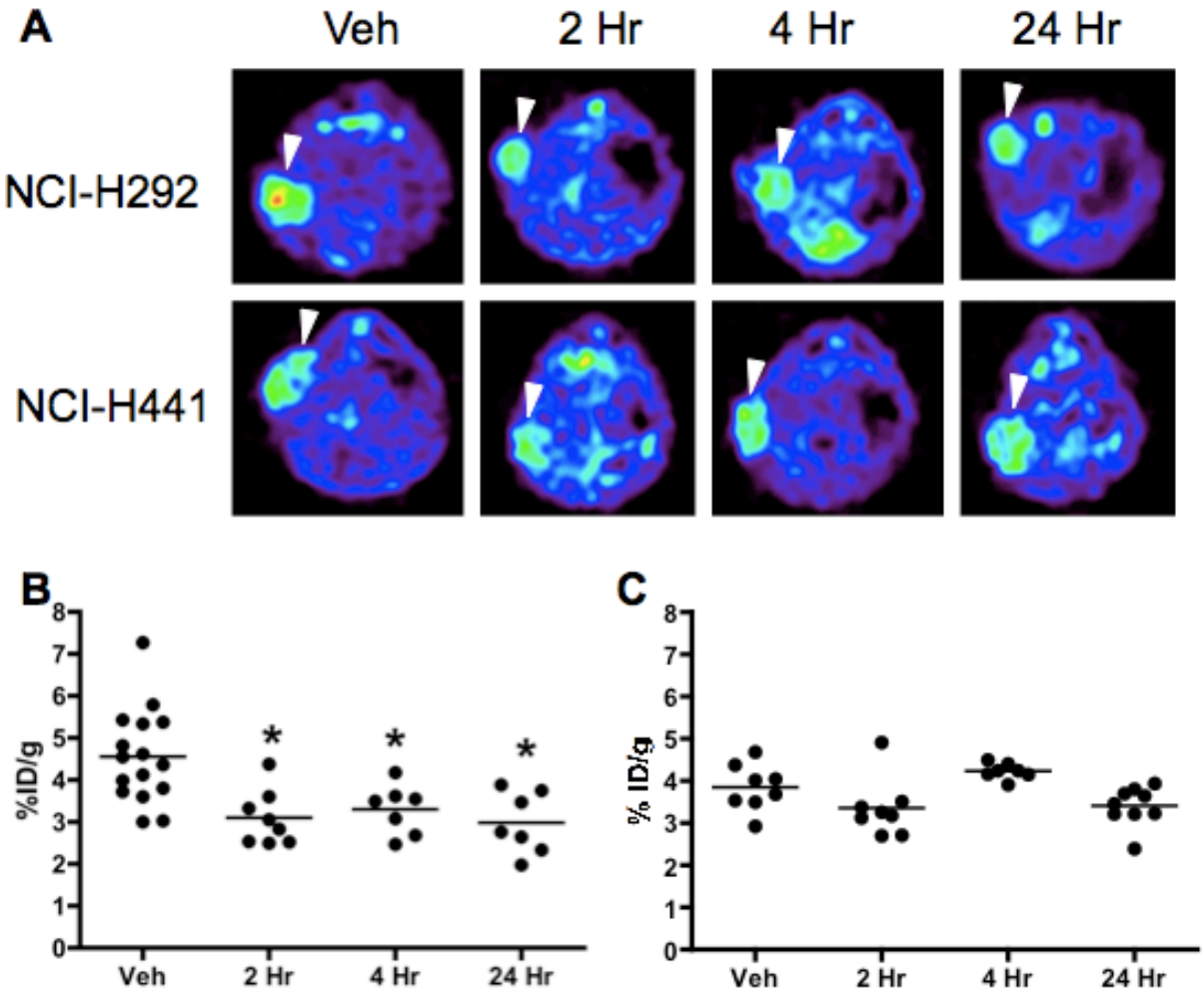


**Fig. 4. *In vivo* $^{18}$FDG-PET.** Representative transverse $^{18}$FDG-PET images of NCI-H292 and NCI-H441 tumor xenografts (A) show that $^{18}$FDG uptake is significantly reduced ($p < 0.05$) in the NCI-H292 xenografts at all time points following a single treatment of 60 mg/kg OSI-906 (B) while NCI-H441 xenografts show no changes in $^{18}$FDG uptake (C).

analogous manner. Figure 2C shows that cytochalasin B significantly inhibits uptake of the radiotracer by 85-90% in this cell line, and that the inhibition of $^{3}$H-2-deoxy glucose by OSI-906 in NCI-H292 cells represents a rapid PD effect.

### II.4.3 Correlation with target-pathway inhibition *in vitro*

NCI-H292 cell lysates were treated with an increasing concentration of OSI-906 (0.0 μM-10 μM) for 30 minutes and then analyzed for pIGF-1R, pIR, pERK 1/2, pAKT,

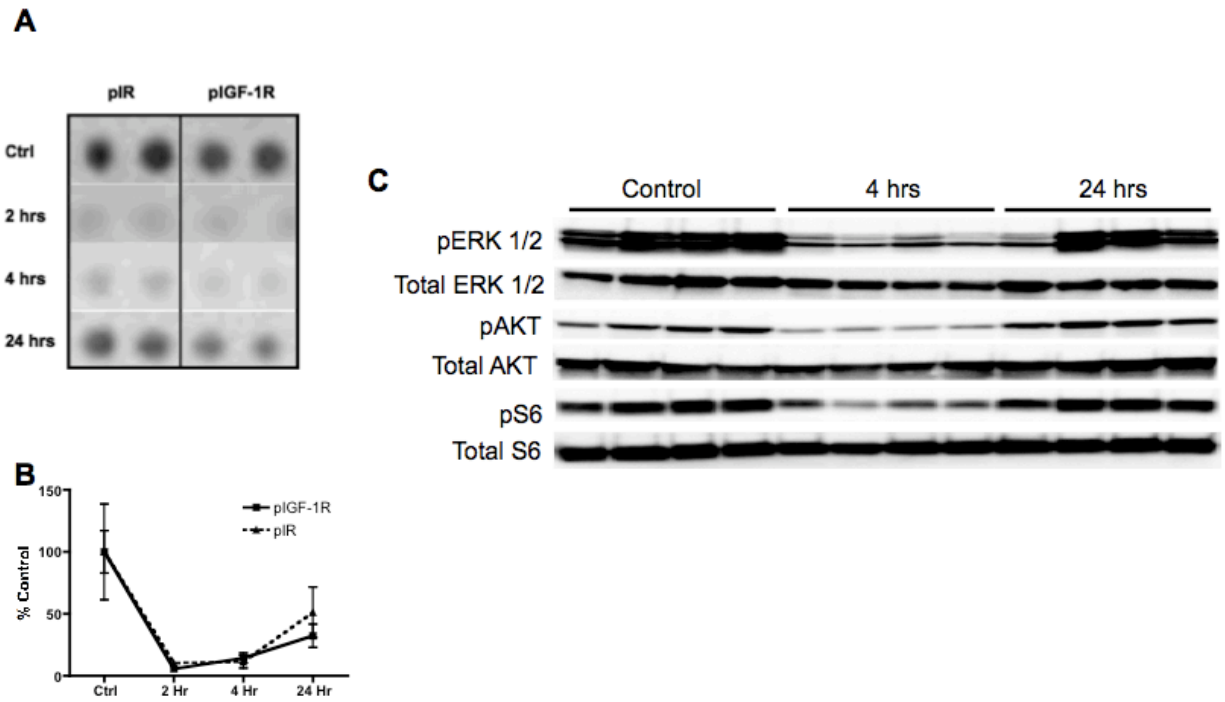


**Fig. 5. *In vivo* biological validation.** RTK array analysis demonstrates strong target inhibition of both pIGF-1R and pIR in NCI-H292 tumor lysates at 2, 4 and 24 hours after a single 60mg/kg treatment of OSI-906 (A,B). *In vivo* Western blot of NCI-H292 tumor lysates at 4 and 24 hours shows inhibition of selected markers of altered glycolysis, pERK 1/2, pAKT and pS6 at 4 hours post-dose that return to baseline levels by 24 hours (C).

pS6 and β-actin as shown in Figure 2D. We observed a significant decrease in phosphorylation of AKT and S6 suggesting a correlation between decreased glucose uptake and inhibition of targets downstream of IGF-1R and IR. NCI-H292 cells treated at lower concentrations (10 nm – 5 μM) over 2, 12 and 24 hours, demonstrated target inhibition at all concentrations at 2 hours, and sustained inhibition of pIGF-1R at both 12 and 24 hours for all concentrations except 10 nM (Fig. 3).

### II.4.4 Inhibition of $^{18}$FDG uptake *in vivo*

$^{18}$FDG-PET images of mice bearing the NCI-H292 and NCI-H441 xenografts are shown in Figure 4A. The NCI-H292 xenografts (sensitive to OSI-906 treatment) show a significant decrease ($p<0.05$) in $^{18}$FDG uptake at 2, 4 and 24 hours post dosing with

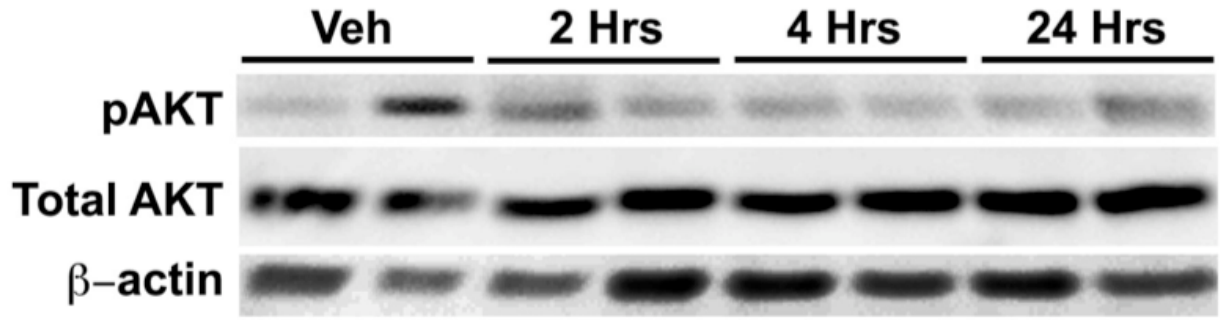


**Fig. 6. *In vivo* Western blot analysis.** *In vivo* Western blot analysis of OSI-906 treated NCI-H441 tumors at 2, 4 and 24 hours shows no significant effect on pAKT levels compared to vehicle treated controls.

OSI-906 compared to vehicle treated controls. NCI-H441 xenografts (insensitive to OSI-906 treatment) did not demonstrate a significant change in uptake of $^{18}$FDG at any time point evaluated. Graphically, these results are shown in Figures 4B and 4C. The decreased %ID/g in the NCI-H292 xenografts is suggestive of a rapid PD effect observed by $^{18}$FDG imaging mediated by the inhibition of IGF-1R and IR pathways by OSI-906. Conversely, for the NCI-H441 xenograft model no difference in uptake of the radiotracer was observed in the tumor samples between vehicle controls and the OSI-906 treatment group.

**II.4.5 Correlation with target pathway inhibition**

Target inhibition of both pIGF-1R and pIR by a single dose of OSI-906 at 60 mg/ kg in vivo in NCI-H292 xenograft tumors is shown in Fig. 5A. The data show that at 2 and 4 hours post treatment target inhibition of pIGF-1R is > 80% with 30% inhibition observed at 24 hours (Fig. 5B). The effect on pIR is equally pronounced, demonstrating significant target inhibition of this receptor. Target inhibition of pIR was > 80% at 4 hours post treatment with 40% inhibition observed at 24 hours. Inhibition of both target receptors correlated with decreased uptake of $^{18}$FDG in the same tumor samples

analyzed. Figure 5C shows the results of a Western blot from tumor lysates at selected time points from mice bearing the NCI-H292 xenografts that were treated with 60mg/kg OSI-906 (n = 4/ group). We found reduced activation levels of targets involved in glycolysis that are downstream of IGF-1R and IR, including pAKT, pS6 and pERK 1/2 as measured four hours post treatment with OSI-906 compared to untreated control lysates. Importantly, Western blot analysis of OSI-906 treated NCI-H441 tumor xenografts which do express very low levels of the target receptor showed no reduction in pAKT levels at any time point compared to control (Fig. 6).

| Time | Plasma Concentration (μM) |
|---|---|
| 2 Hr | 21.48 |
| 4 Hr | 19.58 |
| 8 Hr | 17.49 |
| 24 hr | 6.52 |

**Table 2. Pharmacodynamic analysis of OSI-906 in blood plasma.** Plasma concentrations of OSI-906 in mice at 2, 4, 8 and 24 hours following a single 60 mg/kg dose.

### II.4.6 Pharmacokinetic Analysis

Table 2 shows the drug concentration in the plasma samples from the NCI-H292 xenografts remained at a constant concentration ~20 μM for 2 to 8 hours post dosing. By 24 hours post-dosing, the level of OSI-906 in the plasma had decreased by ~60% to approximately 6.5̣ μM, resulting in some potential loss of target coverage with time.

## II.5 Discussion

Catabolism of glucose through the TCA cycle in normal cells is the preferred method of ATP production leading to cell proliferation and survival. It is now well known that many cancer cells avidly consume glucose and produce lactic acid for ATP

production despite the inefficiency of this metabolic pathway. The reason why cancer cells utilize a less efficient means of ATP production remains elusive; however, recent studies suggest that in cancer cells an increase in glycolysis, in addition to respiration, can generate energy more quickly than normal cells that rely on respiration alone. As a result, this high rate of glucose metabolism by cancer cells has resulted in the wide use of $^{18}$FDG PET to image and diagnose rapidly dividing cells including tumors (22).

Both IGF-1R and IR signal through the PI3K signaling pathway. PI3K is linked to both growth control and glucose metabolism. PI3K directly regulates glucose uptake and metabolism via AKT mediated regulation of glucose transporter activation and expression (GLUT1 and GLUT4), enhanced glucose capture by increased hexokinase activity and stimulation of phosphofructokinase activity (23-26). PI3K activation thus renders cells dependent on glucose leading to glucose addiction. In normal cells, activation of PI3K/AKT is highly controlled by dephosphorylation of phosphatidylinositol by PTEN. However, in many cancers, PTEN is lost leading to constitutive activation of the PI3K pathway (27). Moreover, activation of this pathway can be enhanced by other mechanisms which, when combined, can constitute some of the more prevalent classes of mutations in human malignancy (e.g. PI3CA, AKT2, BCR-ABL, HER2/neu, etc.). Therefore, activation of AKT is likely the most important signaling event in relation to cellular metabolism, because AKT is sufficient to drive glycolysis and lactate formation and suppress macromolecular degradation in cancer (27, 28). It has been shown that various therapeutic agents that disrupt the PI3K/AKT pathway, either directly or upstream of PI3K/AKT lead to decreased glucose uptake in tumors as measured by $^{18}$FDG-PET (29). Furthermore, the ability to inhibit FDG uptake in tumors has been

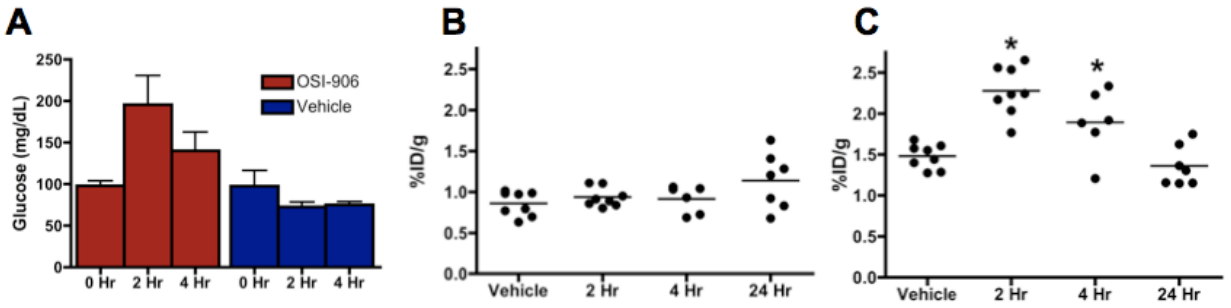


**Fig. 7. Blood glucose measurements.** Blood glucose levels increased at 2 and 4 hours after OSI-906 administration, although levels did not reach statistical significance ($p > 0.05$), compared to baseline. No changes in blood glucose levels were seen in vehicle treated mice over a similar period (A). OSI-906 had no detectable effect on $^{18}$FDG uptake in skeletal muscle (B). $^{18}$FDG uptake in liver was increased at 2 and 4 hours after 60 mg/kg OSI-906 treatment but returned to baseline after 24 hours (C).

shown to correlate well with treatment response in a number of cancers. As a consequence, $^{18}$FDG-PET has been used clinically in cancer patients to predict response to various therapies via the ability of agents to disrupt glucose metabolism and glucose uptake in tumors (26, 30-32).

The primary purpose of these studies was to determine if $^{18}$FDG-PET could be used as an early, non-invasive PD biomarker for the dual kinase inhibitor OSI-906. We first determined in vitro using the sensitive cell line, NCI-H292 that a rapid decrease in $^{3}$H-2-deoxy glucose uptake was observed in a dose dependent manner after treatment with pharmacologically relevant concentrations of OSI-906. In the NCI-H441 cell line reduced sensitivity to equimolar concentrations of OSI-906 was observed for the same assay. NCI-H292 cell lysates were then probed for markers of altered glycolysis by Western blot analysis and showed a significant reduction in pIGF-1R, pIR, pAKT, pS6, and pERK 1/2. Target inhibition of these markers strongly link IGF-1R and IR to the PI3

kinase and AKT pathways and resultant changes in metabolic activity of cultured cells when exposed to OSI-906.

In vivo, decreased uptake of $^{18}$FDG was observed rapidly at 2, 4, and 24 hours after administration of an efficacious dose of 60 mg/kg of OSI-906 in NCI-H292 tumor bearing animals. In comparison, the insensitive NCI-H441 xenografts demonstrated no change in uptake of the radiotracer at the same time points and same dosage. Analysis of target inhibition of pAKT, pS6, pERK 1/2, pIGF-1R and pIR from NCI-H292 tumor lysates was performed by Western blot and RTK array analysis. The results showed strong target inhibition of these markers at 4 hours post administration of a single 60 mg/kg dose of OSI-906, further corroborating the link of metabolic activity of tumors with IGF-1R and IR signaling pathways. Specific target inhibition of pIGF-1R and IR by RTK array analysis resulted in significant ($p < 0.05$) reduction of these phospho-targets (>80%) at 2 and 4 hours post administration of the agent, and correlated to reduced uptake of $^{18}$FDG. Blood glucose levels were elevated from a baseline, fasted level following 2 and 4 hours of 60mg/kg OSI-906 treatment, however, these levels did not reach statistical significance ($p>0.5$). As expected, similarly evaluated vehicle treated mice did not exhibit elevated glucose levels when evaluated at 2 hrs and 4 hrs (Fig. 7A). Importantly, $^{18}$FDG uptake in NCI-H441 tumors, which are insensitive to OSI-906, was similar in both OSI-906-treated and vehicle-treated tumors. The fact that post-treatment $^{18}$FDG uptake in these mice was not decreased when compared to baseline imaging suggests that the somewhat elevated circulating glucose levels had no detectable impact on $^{18}$FDG uptake in this study. As further evidence, no change in $^{18}$FDG uptake was seen in skeletal muscle following OSI-906 (Fig. 7B), and only a slight increase in

liver $^{18}$FDG uptake was seen at 2 and 4 hours before returning to baseline at 24 hours (Fig. 7C).

The present findings support a strong link of rapidly altered metabolic activity in both cultured cells and in vivo tumors induced by target inhibition of the IGF-1R and IR signaling pathways. Though there is still much to be learned how cellular metabolism in proliferating cells is regulated, there is an ever increasing body of information supporting increased communication between signaling pathways and metabolic control of the cell. Thus, $^{18}$FDG-PET should serve as a rapid, non-invasive biomarker of pharmacodynamic effects of OSI-906 in patients treated with this dual IGF-1R/IR kinase inhibitor. This method may be most beneficial in early clinical development where accurate assessment of PD effects is often times limited by the lack of readily accessible tumor samples. As such $^{18}$FDG-PET may be a useful clinical tool in identifying active doses and patients potentially sensitive to this novel antitumor agent and perhaps other compounds of this target class. Currently, $^{18}$FDG-PET imaging is being employed in several clinical trials as a biomarker for early efficacy of OSI-906.

# CHAPTER III

# DISCUSSION

## III.1 Future Work

While $^{18}$FDG-PET was well suited for use in these studies, the complex underlying biology of glucose metabolism may dictate the predilection of other types of probes for certain tumors and treatment types. As such, many new molecular imaging probes are currently being developed. Contemporary molecular imaging research emphasizes the use of new probes to measure biological targets other than glucose metabolism. One such probe is 3'-deoxy-3'[$^{18}$F]-fluorothymidine ($^{18}$FLT), a marker of proliferation (33). $^{18}$FLT is a thymidine analog that when phosphorylated by the cytosolic enzyme Thymidine Kinase 1 (TK1) is trapped inside the cell. We have previously shown that $^{18}$FLT may be a biomarker of response to HER2 targeted therapy in breast cancer while $^{18}$FDG is not (19). However, another study shows that $^{18}$FLT is not a biomarker of response in epidermal growth factor receptor targeted therapy in colorectal cancer (17). These seemingly disparate results have led us to look deeper into the cellular mechanisms of TK1 regulation and will be a large component of our future research. Understanding under what circumstances $^{18}$FDG or $^{18}$FLT would be better suited in imaging treatment response will be of great clinical importance. In addition to $^{18}$FLT, we are developing novel imaging probes for translator protein (TSPO), a trans-mitochondrial membrane protein involved in a number of cellular processes including cholesterol metabolism, steroidogenesis, and apoptosis. Additionally, TSPO expression

levels have been shown to be correlated to tumor grade (34, 35) and patient outcomes across a number of cancer types (36-38). A number of probes have been developed for neuroimaging such as PBR06 (39) and DPA-714 (40). However, until recently these probes have not been evaluated in the context of cancer. In fact, we were the first to show that PBR06 is a promising probe for imaging rat models of glioma (41), and are currently moving forward to preliminary clinical use with these agents. However, all TSPO targeted imaging probes currently in use were not developed for cancer imaging, and the development of a new generation of probes specifically targeting cancer may show significantly better performance than current agents. We have embarked on an ambitious probe discovery project involving the synthesis of hundreds of novel small molecules based upon the PBR06 and DPA-714 parent scaffolds (42). These new ligands are screened by a number of functional assays including radioligand displacement, generation of reactive oxygen species, and steroidogenesis. After screening for desirable properties, the novel ligands are labelled with $^{18}$F for PET imaging in small animals, biological validation and ultimately use in humans. With the development and validation of $^{18}$FLT and TSPO targeted imaging probes we aim to increase the molecular imaging tools available for clinicians beyond $^{18}$FDG to help diagnose disease and direct therapy.

REFERENCES


**1.** Mankoff DA. A definition of molecular imaging. *J Nucl Med.* Jun 2007;48(6):18N, 21N.

**2.** Peterson TE, Manning HC. Molecular imaging: 18F-FDG PET and a whole lot more. *J Nucl Med Technol.* Sep 2009;37(3):151-161.

**3.** Beckmann N. In Vivo magnetic resonance techniques and drug discovery. *Brazilian Journal of Physics.* 2006;36:16-22.

**4.** Casella V, Ido T, Wolf AP, Fowler JS, MacGregor RR, Ruth TJ. Anhydrous F-18 labeled eslemental flurine for radiopharmaceutical preparation. *J Nucl Med.* Aug 1980;21(8):750-757.

**5.** Ji QS, Mulvihill MJ, Rosenfeld-Franklin M, et al. A novel, potent, and selective insulin-like growth factor-I receptor kinase inhibitor blocks insulin-like growth factor-I receptor signaling in vitro and inhibits insulin-like growth factor-I receptor dependent tumor growth in vivo. *Mol Cancer Ther.* Aug 2007;6(8):2158-2167.

**6.** Chan JM, Stampfer MJ, Giovannucci E, et al. Plasma insulin-like growth factor-I and prostate cancer risk: a prospective study. *Science.* Jan 23 1998;279(5350): 563-566.

**7.** Hankinson SE, Willett WC, Colditz GA, et al. Circulating concentrations of insulin-like growth factor-I and risk of breast cancer. *Lancet.* May 9 1998;351(9113): 1393-1396.

**8.** Ma J, Pollak MN, Giovannucci E, et al. Prospective study of colorectal cancer risk in men and plasma levels of insulin-like growth factor (IGF)-I and IGF-binding protein-3. *J Natl Cancer Inst.* Apr 7 1999;91(7):620-625.

**9.** Yu H, Spitz MR, Mistry J, Gu J, Hong WK, Wu X. Plasma levels of insulin-like growth factor-I and lung cancer risk: a case-control analysis. *J Natl Cancer Inst.* Jan 20 1999;91(2):151-156.

**10.** LeRoith D, Roberts CT, Jr. The insulin-like growth factor system and cancer. *Cancer Lett.* Jun 10 2003;195(2):127-137.

**11.** Parker AS, Cheville JC, Janney CA, Cerhan JR. High expression levels of insulin-like growth factor-I receptor predict poor survival among women with clear-cell renal cell carcinomas. *Hum Pathol.* Aug 2002;33(8):801-805.

**12.** Baserga R, Peruzzi F, Reiss K. The IGF-1 receptor in cancer biology. *Int J Cancer.* Dec 20 2003;107(6):873-877.

**13.** Riedemann J, Macaulay VM. IGF1R signalling and its inhibition. *Endocr Relat Cancer.* Dec 2006;13 Suppl 1:S33-43.

**14.** Belfiore A, Frasca F, Pandini G, Sciacca L, Vigneri R. Insulin receptor isoforms and insulin receptor/insulin-like growth factor receptor hybrids in physiology and disease. *Endocr Rev.* Oct 2009;30(6):586-623.

**15.** Buck E, Gokhale P, Koujak S, et al. Compensatory insulin receptor (IR) activation upon inhibition of insulin-like growth factor-1 receptor (IGF-1R): Rationale for co-targeting IGF-1R and IR in cancer. *Mol Cancer Ther.* 2010.

**16.** Mulvihill MJ, Cooke A, Rosenfeld-Franklin M, et al. Discovery of OSI-906: a selective and orally efficacious dual inhibitor of the IGF-1 receptor and insulin receptor. *Future Medicinal Chemistry.* 2009;1(6):1153-1171.

**17.** Manning HC, Merchant NB, Foutch AC, et al. Molecular imaging of therapeutic response to epidermal growth factor receptor blockade in colorectal cancer. *Clin Cancer Res.* Nov 15 2008;14(22):7413-7422.

**18.** Ayers GD, McKinley ET, Zhao P, et al. Volume of preclinical xenograft tumors is more accurately assessed by ultrasound imaging than manual caliper measurements. *J Ultrasound Med.* Jun;29(6):891-901.

**19.** Shah C, Miller TW, Wyatt SK, et al. Imaging biomarkers predict response to anti-HER2 (ErbB2) therapy in preclinical models of breast cancer. *Clin Cancer Res.* Jul 15 2009;15(14):4712-4721.

**20.** Fueger BJ, Czernin J, Hildebrandt I, et al. Impact of animal handling on the results of 18F-FDG PET studies in mice. *J Nucl Med.* Jun 2006;47(6):999-1006.

**21.** Dandekar M, Tseng JR, Gambhir SS. Reproducibility of 18F-FDG microPET studies in mouse tumor xenografts. *J Nucl Med.* Apr 2007;48(4):602-607.

**22.** Weber WA. Positron emission tomography as an imaging biomarker. *J Clin Oncol.* Jul 10 2006;24(20):3282-3292.

**23.** Elstrom RL, Bauer DE, Buzzai M, et al. Akt stimulates aerobic glycolysis in cancer cells. *Cancer Res.* Jun 1 2004;64(11):3892-3899.

**24.** Clemmons DR. Involvement of insulin-like growth factor-I in the control of glucose homeostasis. *Curr Opin Pharmacol.* Dec 2006;6(6):620-625.

**25.** Deberardinis RJ, Sayed N, Ditsworth D, Thompson CB. Brick by brick: metabolism and tumor cell growth. *Curr Opin Genet Dev.* Feb 2008;18(1):54-61.

**26.** Vander Heiden MG, Cantley LC, Thompson CB. Understanding the Warburg effect: the metabolic requirements of cell proliferation. *Science.* May 22 2009;324(5930): 1029-1033.

**27.** DeBerardinis RJ, Lum JJ, Hatzivassiliou G, Thompson CB. The biology of cancer: metabolic reprogramming fuels cell growth and proliferation. *Cell Metab.* Jan 2008;7(1):11-20.

**28.** Kroemer G, Pouyssegur J. Tumor cell metabolism: cancer's Achilles' heel. *Cancer Cell.* Jun 2008;13(6):472-482.

**29.** Engelman JA, Chen L, Tan X, et al. Effective use of PI3K and MEK inhibitors to treat mutant Kras G12D and PIK3CA H1047R murine lung cancers. *Nat Med.* Dec 2008;14(12):1351-1356.

**30.** DeBerardinis RJ. Is cancer a disease of abnormal cellular metabolism? New angles on an old idea. *Genet Med.* Nov 2008;10(11):767-777.

**31.** Kelloff GJ, Hoffman JM, Johnson B, et al. Progress and promise of FDG-PET imaging for cancer patient management and oncologic drug development. *Clin Cancer Res.* Apr 15 2005;11(8):2785-2808.

**32.** Mankoff DA, Eary JF, Link JM, et al. Tumor-specific positron emission tomography imaging in patients: [18F] fluorodeoxyglucose and beyond. *Clin Cancer Res.* Jun 15 2007;13(12):3460-3469.

**33.** Shields AF, Grierson JR, Dohmen BM, et al. Imaging proliferation in vivo with [F-18]FLT and positron emission tomography. *Nat Med.* Nov 1998;4(11): 1334-1336.

**34.** Vlodavsky E, Soustiel JF. Immunohistochemical expression of peripheral benzodiazepine receptors in human astrocytomas and its correlation with grade of malignancy, proliferation, apoptosis and survival. *J Neurooncol.* Jan 2007;81(1): 1-7.

**35.** Deane NG, Manning HC, Foutch AC, et al. Targeted imaging of colonic tumors in smad3-/- mice discriminates cancer and inflammation. *Mol Cancer Res.* Apr 2007;5(4):341-349.

**36.** Maaser K, Grabowski P, Sutter AP, et al. Overexpression of the peripheral benzodiazepine receptor is a relevant prognostic factor in stage III colorectal cancer. *Clin Cancer Res.* Oct 2002;8(10):3205-3209.

**37.** Miettinen H, Kononen J, Haapasalo H, et al. Expression of peripheral-type benzodiazepine receptor and diazepam binding inhibitor in human astrocytomas: relationship to cell proliferation. *Cancer Res.* Jun 15 1995;55(12):2691-2695.

**38.** Han Z, Slack RS, Li W, Papadopoulos V. Expression of peripheral benzodiazepine receptor (PBR) in human tumors: relationship to breast, colorectal, and prostate tumor progression. *J Recept Signal Transduct Res.* 2003;23(2-3):225-238.

**39.** Imaizumi M, Briard E, Zoghbi SS, et al. Kinetic evaluation in nonhuman primates of two new PET ligands for peripheral benzodiazepine receptors in brain. *Synapse.* Aug 2007;61(8):595-605.

**40.** James ML, Fulton RR, Vercoullie J, et al. DPA-714, a new translocator protein-specific ligand: synthesis, radiofluorination, and pharmacologic characterization. *J Nucl Med.* May 2008;49(5):814-822.

**41.** Buck JR, McKinley ET, Hight MR, et al. Quantitative, preclinical PET of translocator protein expression in glioma using 18F-N-fluoroacetyl-N-(2,5-dimethoxybenzyl)-2-phenoxyaniline. *J Nucl Med.* Jan;52(1):107-114.

**42.** Tang D, Buck JR, Hight MR, Manning HC. Microwave-assisted Organic Synthesis of a High-affinity Pyrazolo-pyrimidinyl TSPO Ligand. *Tetrahedron Lett.* Sep 1;51 (35):4595-4598.